

Anisotropic plasmon dispersion and damping inmultilayer 8-*Pmmn* borophene structures

Kejian Liu(刘可鉴), Jian Li(李健), Qing-Xu Li(李清旭), and Jia-Ji Zhu(朱家骥)

Citation: Chin. Phys. B, 2022, 31 (**11**): 117303. DOI: 10.1088/1674-1056/ac6b2d

What follows is a list of articles you may be interested in

Light focusing in linear arranged symmetric nanoparticle trimer on metal film system

Yuxia Tang(唐裕霞), Shuxia Wang(王蜀霞), Yingzhou Huang(黄映洲), and Yurui Fang(方蔚瑞)

Chin. Phys. B, 2022, 31 (**1**): 017303. DOI: 10.1088/1674-1056/ac20c3

First-principles study of plasmons in doped graphene nanostructures

Xiao-Qin Shu(舒晓琴), Xin-Lu Cheng(程新路), Tong Liu(刘彤), and Hong Zhang(张红)

Chin. Phys. B, 2021, 30 (**9**): 097301. DOI: 10.1088/1674-1056/abe92d

Collective excitations and quantum size effects on the surfaces of Pb(111) films: An experimental study

Yade Wang(王亚德), Zijian Lin(林子荐), Siwei Xue(薛思玮), Jiade Li(李佳德), Yi Li(李毅), Xuetao Zhu(朱学涛), and Jiandong Guo(郭建东)

Chin. Phys. B, 2021, 30 (**7**): 077308. DOI: 10.1088/1674-1056/abfbcd

Quantifying plasmon resonance and interband transition contributions in photocatalysis of gold nanoparticle

Liang Dong(董亮), Chengyun Zhang(张成云), Lei Yan(严蕾), Baobao Zhang(张宝宝), Huan Chen(陈环), Xiaohu Mi(弥小虎), Zhengkun Fu(付正坤), Zhenglong Zhang(张正龙), and Hairong Zheng(郑海荣)

Chin. Phys. B, 2021, 30 (**7**): 077301. DOI: 10.1088/1674-1056/abfa0c

High sensitive chiral molecule detector based on the amplified lateral shift in Kretschmann configuration involving chiral TDBCs

Song Wang(王松), Qihui Ye(叶起惠), Xudong Chen(陈绪栋), Yanzhu Hu(胡燕祝), and Gang Song(宋钢)

Chin. Phys. B, 2021, 30 (**6**): 067301. DOI: 10.1088/1674-1056/abdda6

Anisotropic plasmon dispersion and damping in multilayer 8-*Pmmn* borophene structures

Kejian Liu(刘可鉴)[1], Jian Li(李健)[1,2,3], Qing-Xu Li(李清旭)[1,2], and Jia-Ji Zhu(朱家骥)[1,2,3,†]

[1] *School of Science, Chongqing University of Posts and Telecommunications, Chongqing* 400065, *China*
[2] *Institute for Advanced Sciences, Chongqing University of Posts and Telecommunications, Chongqing* 400065, *China*
[3] *Southwest Center for Theoretical Physics, Chongqing University, Chongqing* 401331, *China*

(Received 2 April 2022; accepted manuscript online 28 April 2022)

We investigate the collective plasma oscillations theoretically in multilayer 8-*Pmmn* borophene structures, where the tilted Dirac electrons in spatially separated layers are coupled via the Coulomb interaction. We calculate the energy dispersions and Landau dampings of the multilayer plasmon excitations as a function of the total number of layers, the interlayer separation, and the different orientations. Like multilayer graphene, the plasmon spectrum in multilayer borophene consists of one in-phase optical mode and $N-1$ out-of-phase acoustical modes. We show that the plasmon modes possess kinks at the boundary of the interband single-particle continuum and the apparent anisotropic behavior. All the plasmon modes approach the same dispersion at a sufficiently large interlayer spacing in the short-wavelength limit. Especially along specific orientations, the optical mode could touch an energy maximum in the nondamping region, which shows non-monotonous behavior. Our work provides an understanding of the multilayer borophene plasmon and may pave the way for multilayer borophene-based plasmonic devices.

Keywords: plasmon, 8-*Pmmn* borophene, multilayer, two-dimensional materials

PACS: 73.20.Mf, 78.67.Pt, 73.21.Ac, 68.65.−k **DOI:** 10.1088/1674-1056/ac6b2d

1. Introduction

Graphene and the booming two-dimensional (2D) materials have been the superstars for their novel properties in condensed matter physics since 2004.[1] Now the 2D materials include not only graphene and the derivatives of graphene but also transition metal dichalcogenides (TMDs),[2–7] black phosphorus,[8–12] indium selenide,[13] stanene,[14–17] and many other layered materials.[18–23] Due to various advantages of the 2D materials, such as long lifetime,[24] gate tunability,[25,26] and optoelectronic applications,[2,27] they become promising materials for a wide range of nanophotonics and optoelectronics.[25,28–30]

Plasmon, the elementary excitation of the interacting electron/hole gas, with novel plasmonic phenomena like selective absorbance and scattering, subwavelength bound state, and local field enhancement, plays a fundamental role in researching the dielectric and optical properties of metals and semiconductors.[31] Resulting from the unusual linear dispersion of the Dirac massless electrons, graphene plasmons show the exceptional properties of electrical tunability, low intrinsic loss, and high optical field localization. In recent years, plenty of graphene-based plasmonic devices have been proposed theoretically and demonstrated experimentally, such as photodetectors,[32,33] terahertz lasers,[34] resonators,[35] and biosensors.[36–38] Along with graphene, plasmons in the other 2D materials, e.g., MoS_2,[39] WTe_2,[40] 2H-$TaSe_2$,[41] and phosphorene[42,43] also attracted more and more interests.

Several 2D boron structures have been predicted and experimentally fabricated.[44,45] As one of the most stable structures, the 8-*Pmmn* borophene, an orthorhombic lattice with three-mirror symmetry planes perpendicular to each other and a glide plane at one of the mirror symmetry planes,[46,47] belongs to the space group *Pmmn* (No. 59 in Ref. [48]). The 8-*Pmmn* borophene reveals the tilted Dirac cone and anisotropic massless Dirac fermions by first-principles calculations,[49,50] which sharply contrasts the up-right Dirac cone and isotropic Dirac fermions in graphene. There have been reported that plasmon dispersion possesses the anisotropic behavior[51] and the tilt-induced kink[52,53] in 8-*Pmmn* borophene. However, the dependence on electron concentration of both the plasmonic resonance frequency and magnitude is relatively weak in monolayer 8-*Pmmn* borophene, limiting its applications in nanophotonics. One may expect the transparent photonic devices based on 8-*Pmmn* borophene/insulator stacks by depositing alternating wafer-scale borophene sheets and thin insulating layers, which could be grouped into photonic-crystal-like structures.

This paper presents a detailed study of the multilayer optical and acoustical dispersion in 8-*Pmmn* borophene. Within the quantum theory of the electron liquid, based on the matrix Dyson equation for the Coulomb propagator in multilayer borophene, we calculate the dispersion and Landau damping of plasmons and understand their dependence on the in-layer electron density, number of layers, and interlayer spacing. The plasmon spectra consist of one optical mode with a square-root dispersion and $N-1$ acoustical modes with linear dispersion. We show that the plasmon modes possess kinks at the boundary of the interband single-particle continuum, and the Lan-

†Corresponding author. E-mail: zhujj@cqupt.edu.cn
© 2022 Chinese Physical Society and IOP Publishing Ltd

dau damping drastically increases within the interband single-particle continuum. All the plasmon modes approach the same dispersion at a sufficiently large interlayer spacing in the short-wavelength limit. The plasmons in multilayer borophene show the apparent anisotropic behavior, and the optical mode could touch an energy maximum in the nondamping region along specific orientations.

2. Model

The Hamiltonian of 8-*Pmmn* borophene is given by[54,55]

$$H_0 = \left(v_x\sigma_x p_x + v_y\sigma_y p_y + \eta v_y \sigma_0 p_y\right), \tag{1}$$

where $p_{x,y}$ are the momentum operators, $\sigma_{x,y}$ are 2×2 Pauli matrices, and σ_0 is a 2×2 identity matrix. The anisotropic velocities are $v_x = 0.86\times 10^6$ m/s, $v_y = 0.69\times 10^6$ m/s, and $\eta = 0.46$ is the tilt parameter of Dirac cone.[54] The energy dispersion and corresponding wave functions of monolayer 8-*Pmmn* borophene are given by

$$\varepsilon_{s\boldsymbol{k}} = \hbar\eta v_y k_y + s\hbar\sqrt{v_x^2 k_x^2 + v_y^2 k_y^2}, \tag{2}$$

$$\psi_{s,\boldsymbol{k}} = \frac{1}{\sqrt{2}}\begin{pmatrix} 1 \\ s\mathrm{e}^{\mathrm{i}\theta_k}\end{pmatrix}, \tag{3}$$

where $s = +(-)$ is the band index for conduction (valance) band and θ_k is the polar angle of the wave vector $\boldsymbol{k}$ respect to x-axis. Since the Dirac cone is tilted and the Fermi surface is not a circle but an ellipse, we define the Fermi vector k_{F} by letting the area of the elliptic Fermi surface the same as the area of a circle whose radius is k_{F}. The Fermi energy ε_{F} can be expressed by the effective Fermi vector k_{F} as[56]

$$\varepsilon_{\mathrm{F}} = \hbar\left(v_x v_y\right)^{\frac{1}{2}} k_{\mathrm{F}}\left(1-\eta^2\right)^{\frac{3}{4}}. \tag{4}$$

The tilted Dirac cone reduces to up-right Dirac cone (e.g., the case of graphene) when $\eta = 0$ and $v_x = v_y = v_{\mathrm{F}}$.

We consider the structure of multilayer 8-*Pmmn* borophene with interlayer spacing d as shown in Fig. 1. The bare Coulomb interaction is a symmetric tensor

$$v_{ij}(q) = v_q \exp\left(-|i-j|qd\right) \tag{5}$$

with respect to the layer indices $i = j = 1, 2, \ldots, N$. The off-diagonal (diagonal) elements represents the interlayer (intralayer) Coulomb interaction and $v_q = 2\pi e^2/(\kappa q)$ is the Fourier transform of intralayer Coulomb interaction with κ being the static dielectric constant. Here we assume that the dielectric background of the environment surrounding borophene layers is homogeneous and can be well described by an average effective dielectric constant. Since the effective dielectric constant does not alter the dispersion of plasmon qualitatively, we can take the effective dielectric constant as 1, which merely means a renormalization of unit.[52]

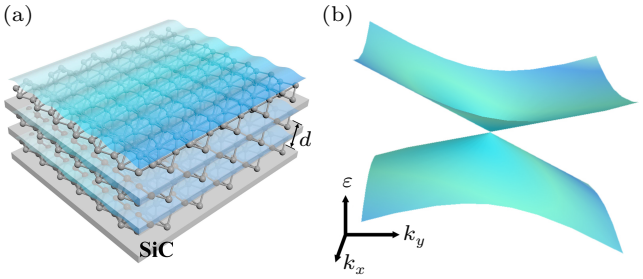


Fig. 1. Schematic diagram of plasmon for N-layer 8-*Pmmn* borophene. (b) The tilted and anisotropic Dirac cone in 8-*Pmmn* borophene.

Within a practical setup, the interlayer spacing of d multilayer 8-*Pmmn* borohpene should be sufficiently large so that the electron tunneling between layers is neglectable. Therefore, only the diagonal elements of the polarizability remains and $\Pi(q,\omega) = \delta_{ij}\Pi^i(q,\omega)$.

The noninteracting Lindhard polarization function of each layer of 8-*Pmmn* borophene is given by

$$\Pi^i(\boldsymbol{q},\omega) = \frac{g}{L^2}\sum_{\boldsymbol{k},s,s'}\frac{n_{s\boldsymbol{k}} - n_{s'\boldsymbol{k}+\boldsymbol{q}}}{\hbar\omega^+ + \varepsilon_{s\boldsymbol{k}} - \varepsilon_{s'\boldsymbol{k}+\boldsymbol{q}}} f_{ss'}(\boldsymbol{k},\boldsymbol{q}), \tag{6}$$

where $g = 2$ is the degeneracy from spin, $n_{s\boldsymbol{k}}$ represents Fermi function which reduces to step function in zero temperature and $\omega^+ = \omega + \mathrm{i}\delta$ with $\delta\to 0$. From the wave functions of the 8-*Pmmn* borophene, the overlap function is given by

$$f_{ss'}(\boldsymbol{k},\boldsymbol{q}) = \frac{1}{2}\left(1 + ss'\cos\theta_{kk'}\right), \tag{7}$$

where $\theta_{kk'} = \theta_k - \theta_{k+q}$, θ_q and θ_{k+q} are the polar angle of wave vector $\boldsymbol{q}$ and $\boldsymbol{k}+\boldsymbol{q}$, respectively.

The dynamical polarization function of monolayer borophene can be calculated by[52]

$$\begin{aligned}\mathrm{Re}\Pi^i(\boldsymbol{q},\omega) = {} & \frac{g}{4\pi^2\hbar^2 v_x v_y}\left\{-\frac{\pi^2 q^2}{4}\frac{\Theta(q-|\Omega|)}{\sqrt{q^2-\Omega^2}} + \int \mathrm{d}\theta\int_0^{\mu/(1+\eta\cos\theta_k)} k\,\mathrm{d}k\,\frac{(\Omega+k)+k'\cos\theta_{kk'}}{(\Omega+k)^2-(k')^2}\right. \\ & \left. + \int \mathrm{d}\theta\int_0^{\mu/(1-\eta\cos\theta_k)}\frac{(-\Omega+k)+k'\cos\theta_{kk'}}{(-\Omega+k)^2-(k')^2}\right\},\end{aligned} \tag{8}$$

$$\begin{aligned}\mathrm{Im}\Pi^i(\boldsymbol{q},\omega) = {} & -\frac{gq^2}{16\hbar^2 v_x v_y}\frac{\mathrm{sgn}(\Omega)}{\sqrt{\Omega^2-q^2}}\Theta(\Omega-q) - \frac{g}{8\pi\hbar v_x v_y}\sum_{\boldsymbol{k}}\Theta(\mu-k-k\eta\cos\theta_k) \\ & \times\left(\left(1+\cos(\theta_k-\theta_{k'})\right)\delta\left(\Omega+k-k'\right) + \left(1-\cos(\theta_k-\theta_{k'})\right)\delta\left(\Omega+k+k'\right)\right) \\ & -\Theta(\mu-k+k\eta\cos\theta_k)\left(\left(1+\cos(\theta_k-\theta_{k'})\right)\delta\left(-\Omega+k-k'\right) + \left(1-\cos(\theta_k-\theta_{k'})\right)\delta\left(-\Omega+k+k'\right)\right),\end{aligned} \tag{9}$$

where $\Omega = \hbar\omega - \hbar v_x q\eta\cos\theta_q$. Note that we have already assumed that the dielectric background is homogeneous. Then the plasmon dispersion can be calculated by the evaluating zeros of the dynamical dielectric function $\varepsilon(\boldsymbol{q},\omega)$, i.e.,

$$\mathrm{Re}\varepsilon(\boldsymbol{q},\omega) = 0 \tag{10}$$

with

$$\varepsilon(\boldsymbol{q},\omega) = \Pi_{i=1}^{N}\left[1 - f_N^i(qd)\, v(q)\, \Pi^i(\boldsymbol{q},\omega)\right] = 0, \tag{11}$$

where $f_N^i(qd)$ is the plasmon mode relation as N $(i=1)$ or $\alpha_N^i qd$ $(i\neq 1)$. The coefficient α_N^i determines the velocity of the ith acoustic plasmon mode.

The Landau damping function of plasmon modes can be well described by the broadening function of the respective plasmon dispersion[57]

$$\Gamma_i(\boldsymbol{q}) = \Gamma(\boldsymbol{q},\omega)|_{\omega=\omega_i(q)}, \tag{12}$$

where the function

$$\Gamma(\boldsymbol{q},\omega) = \frac{\mathrm{Im}\Pi^i(\boldsymbol{q},\omega)}{\partial\mathrm{Re}\Pi^i(\boldsymbol{q},\omega)/\partial\omega} \tag{13}$$

gives the damping of plasmons due to the properties of the intra/interband single-particle continuum.

3. Results and discussion

In the following paragraphs, we present our numerical results for the energy dispersion and Landau damping of multilayer 8-*Pmmn* borophene with the different number of layers N, interlayer separation d and polar angle θ_q. We calculate the energy spectrum from the general formula (10). In all figures, we adopt the units ε_F and k_F for plasmon energy and momentum, respectively. For the electron density $n = 10^{12}$ cm^{-2}, we have $\varepsilon_\mathrm{F} = 106$ meV and $k_\mathrm{F} = 2.507\times10^6$ cm^{-1} .

In Fig. 2, we plot the plasmon dispersion of N-layer 8-*Pmmn* borophene with $N = 2$, 3, 4, and 5, $d = 2$ nm and $\theta_q = \pi/5$. The plasmon dispersion in a monolayer is shown by a black dashed line for reference. There are two kinds of plasmon modes in N-layer 8-*Pmmn* borophene, one in-phase optical mode and $N-1$ out-of-phase acoustical modes. The in-phase optical mode shifts to higher energies when the number of layers increases. With increasing N, the number of the multilayer acoustical modes increases correspondingly, and the energy of upper-lying modes enhances. In contrast, the lowest-lying mode approaches the single-particle continuum boundary. The enhancement enables the top acoustical mode to cross the monolayer mode of five-layer borophene in the interband single-particle continuum. Notice that only two of the four acoustical modes are suppressed in five-layer compared with the acoustical mode in double-layer. In the short-wavelength limit, the behavior of multilayer plasmon modes shows a dramatic difference, which is in sharp contrast to graphene.[57] The optical mode has a kink at the boundary between the interband single-particle continuum and the nondamping region. However, the acoustical modes show rather faint evidence of the kink.

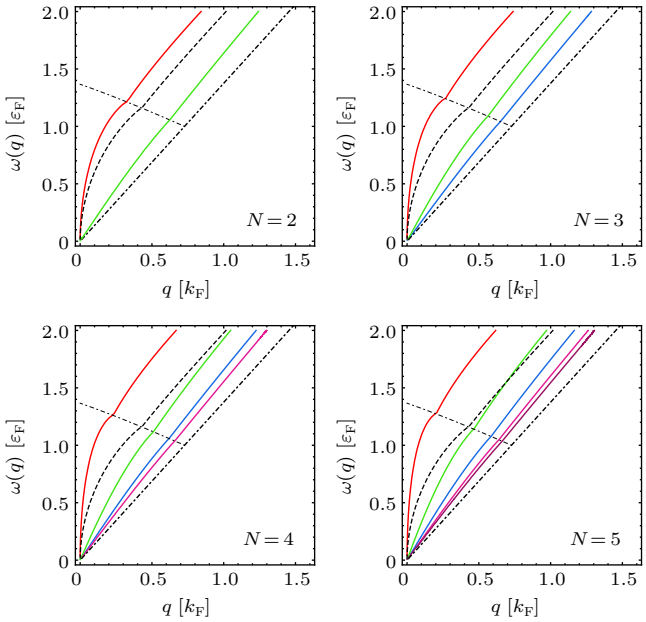


Fig. 2. Plasmon dispersion for N-layer ($N = 2$, 3, 4, 5) 8-*Pmmn* borophene with $d = 2$ nm, $n = 10^{12}$ cm^{-2} and $\theta_q = \pi/5$. The black dot-dashed line show the boundaries of intra- and inter-band single-particle continuum. Black dashed line is plasmon mode in monolayer 8-*Pmmn* borophene. Color solid line represent the plasmon modes.

In Fig. 3, we study the Landau damping of the corresponding multilayer plasmon modes shown in Fig. 2. The energy enhancement for all multilayer modes results in a more extensive broadening of the corresponding plasmon dispersion, which dues to the increasing distance of the plasmon modes from the boundary of the intraband single-particle continuum. The Landau damping also shows the kink at the momentum corresponding to the boundary between the nondamping region and interband single-particle continuum, similar to the plasmon dispersion. The damping increases drastically in the interband single-particle continuum, which is in agreement with a previous study about the loss function of plasmons in monolayer borophene.[52]

In Fig. 4, we study the plasmon dispersion of three-layer borophene with various interlayer separations d. The most apparent behavior is that the energy of in-phase optical mode decreases while the energies of out-of-phase acoustical modes increase with increasing d. However, all multilayer plasmon modes in the short-wavelength limit remain almost the same when the interlayer spacing is sufficiently large (e.g., $d = 10$ nm), which reproduces the result in graphene multilayer.[57] This means all multilayer modes for $q \gg k_\mathrm{F}$ coagulate around the monolayer plasmon mode independent of the number of layers if the interlayer separation is large enough. The physical reason lies in that the influence of the interlayer tunneling vanishes, and the plasmon branches from

different layers behave independently. However, the kink of the optical mode is robust against the increasing interlayer separation. In contrast, the acoustical modes develop rather faint kinks on the boundary of the interband single-particle continuum.

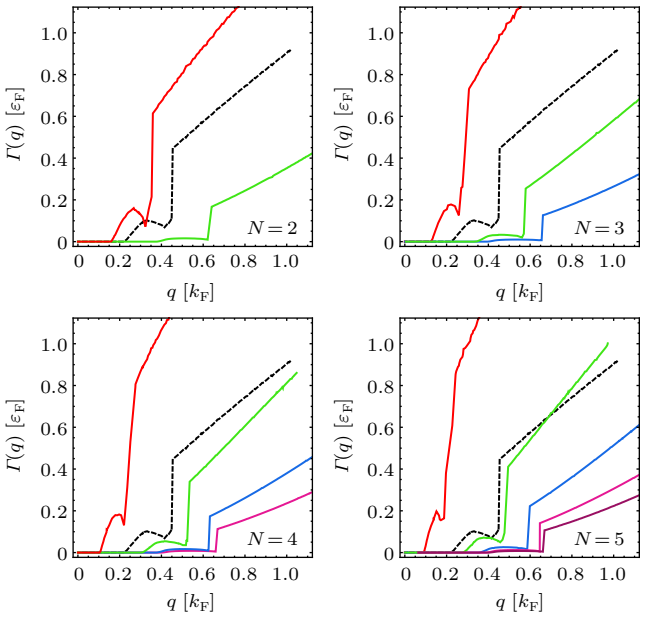


Fig. 3. The damping function for N-layer (N = 2, 3, 4, 5) 8-*Pmmn* borophene with d = 2 nm, $n = 10^{12}$ cm^{-2} and $\theta_q = \pi/5$. Black dashed line shows the Landau damping function in monolayer 8-*Pmmn* borophene. Color solid line represents the Landau damping function.

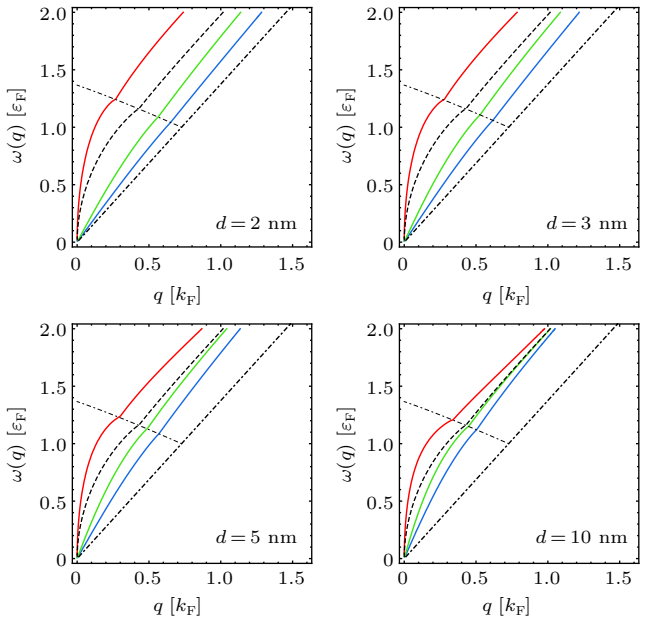


Fig. 4. Plasmon dispersion for threelayer 8-*Pmmn* borophene with $n = 10^{12}$ cm^{-2} and $\theta_q = \pi/5$. Under the condition of d = 2 nm, 3 nm, 5 nm, 10 nm. All other parameters and notations are the same as plasmon mode in Fig. 2.

Figure 5 shows the anisotropic spectra of the three-layer plasmon modes with different polar angle θ_q ($\theta_q = n\pi/5$, n = 0, 1, 3, and 5). We can find that the plasmon modes possess different behavior in different directions. Compared with the case of $\theta_q = 0$, the boundary of the intraband single-particle continuum is pushed down, and the energy of the plasmon modes decreases out of the long-wavelength limit. As θ_q increases from 0 to π, the kinks become more and more apparent, especially for the acoustical modes. Note that the optical mode touches an energy maximum in the nondamping region, and the acoustical modes tend to behave like the optical mode when the θ_q approaches π. These anisotropic plasmons are caused by strong tilt Dirac dispersion of 8-*Pmmn* borophene.

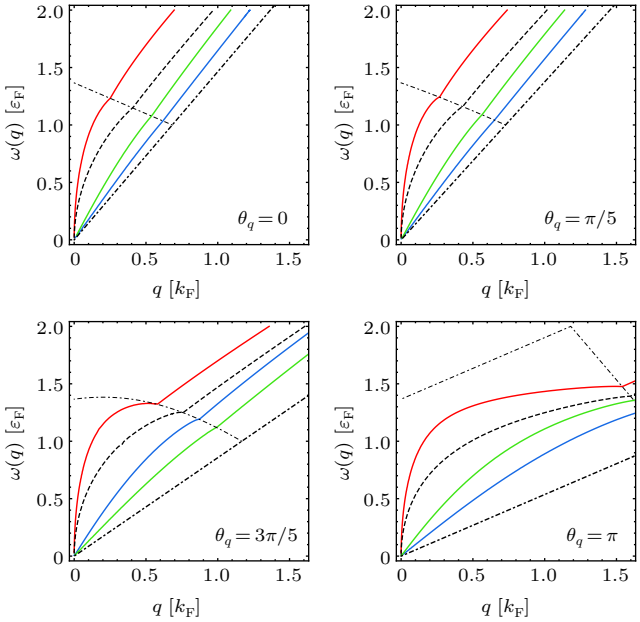


Fig. 5. Plasmon dispersion for three-layer 8-*Pmmn* borophene with $n = 10^{12}$ cm^{-2} and d = 2 nm. (a)–(d) correspond to directions $\theta_q = n\pi/5$, with n = 0, 1, 3, 5. All other parameters and notations are the same as plasmon mode in Fig. 2.

4. Summary

In this paper, we have investigated the collective plasma oscillations theoretically in multilayer 8-*Pmmn* borophene structures, where anisotropic and tilted Dirac electrons in spatially separated layers are coupled via the Coulomb interaction. We calculated the energy dispersions and Landau dampings of the multilayer plasmon excitations as a function of the total number of layers N, the interlayer separation d, and the polar angle θ_q. The multilayer plasmon spectrum consists of one in-phase optical mode and $N-1$ out-of-phase acoustical modes. The energy of the in-phase branch and upper-lying out-of-phase branches of the multilayer plasmon increase with increasing the number of 8-*Pmmn* borophene layers, while the other branches decrease. The optical mode has an apparent kink at the boundary of the interband single-particle continuum, but the acoustical modes show rather faint evidence of their kinks. The Landau damping also shows a similar kink at the boundary and drastically increases within the interband single-particle continuum. As the interlayer separation d increases, all the plasmon modes approach the same dispersion in the short-wavelength limit and sufficiently large interlayer spacing. We also show the anisotropic behavior of the plasmon

in multilayer borophene. The optical in-phase mode touches an energy maximum in the nondamping region, and the linear dispersion of the acoustical out-of-phase modes becomes square-root dispersion when the θ_q approaches π. The presented numerical calculations provide an understanding of the multilayer borophene plasmon depending on the tunable parameters. Our work may pave a way for the plasmonic devices based on multilayer 8-*Pmmn* borophene.

Acknowledgments

This work was supported by the Scientific Research Program from Science and Technology Bureau of Chongqing City (Grant No. cstc2020jcyj-msxmX0684), the Science and Technology Research Program of Chongqing Municipal Education Commission (Grant No. KJQN202000639), and in part by the National Natural Science Foundation of China (Grant No. 12147102).

References

[1] Novoselov K S, Geim A K, Morozov S V, Jiang D, Zhang Y S, Dubonos S V, Grigorieva I V and Firsov A A 2004 *Science* **306** 666
[2] Wang Q H, Kalantar-Zadeh K, Kis A, Coleman J N and Strano M S 2012 *Nat. Nanotechnol.* **7** 699
[3] Mak K F, Lee C, Hone J, Shan J and Heinz T F 2010 *Phys. Rev. Lett.* **105** 136805
[4] Chhowalla M, Shin H S, Eda G, Li L J, Loh K P and Zhang H 2013 *Nat. Chem.* **5** 263
[5] Cao T, Wang G, Han W P, Ye H Q, Zhu C R, Shi J R, Niu Q, Tan P H, Wang E G, Liu B L and Feng J 2012 *Nat. Commun.* **3** 887
[6] Coleman J N, Lotya M, O'Neill A, Bergin S D, King P J, Khan U, Young K, Gaucher A, De S, Smith R J, *et al.* 2011 *Science* **331** 568
[7] Radisavljevic B, Radenovic A, Brivio J, Giacometti V and Kis A 2011 *Nat. Nanotechnol.* **6** 147
[8] Li L K, Yu Y J, Ye G J, Ge Q Q, Ou X D, Wu H, Feng D L, Chen X H and Zhang Y 2014 *Nat. Nanotechnol.* **9** 372
[9] Qiao J S, Kong X H, Hu Z X, Yang F and Ji W 2014 *Nat. Commun.* **5** 4475
[10] Xia F N, Wang H and Jia Y C 2014 *Nat. Commun.* **5** 4458
[11] Tran V, Soklaski R, Liang Y F and Yang L 2014 *Phys. Rev. B* **89** 235319
[12] Rodin A S, Carvalho A and Castro Neto A H 2014 *Phys. Rev. Lett.* **112** 176801
[13] Ding W J, Zhu J B, Wang Z, Gao Y F, Xiao D, Gu Y, Zhang Z Y and Zhu W G 2017 *Nat. Commun.* **8** 14956
[14] Zhu F F, Chen W J, Xu Y, Gao C L, Guan D D, Liu C H, Qian D, Zhang S C and Jia J F 2015 *Nat. Mater.* **14** 1020
[15] Deng J L, Xia B Y, Ma X C, Chen H Q, Shan H, Zhai X F, Li B, Zhao A D, Xu Y, Duan W H, Zhang S C, Wang B and Hou J G 2018 *Nat. Mater.* **17** 1081
[16] Liao M H, Zang Y Y, Guan Z Y, Li H W, Gong Y, Zhu K J, Hu X P, Zhang D, Xu Y, Wang Y Y, He K, Ma X C, Zhang S C and Xue Q K 2018 *Nat. Phys.* **14** 344
[17] Rachel S and Ezawa M 2014 *Phys. Rev. B* **89** 195303
[18] Reis F, Li G, Dudy L, Bauernfeind M, Glass S, Hanke W, Thomale R, Schäfer J and Claessen R 2017 *Science* **357** 287
[19] Aktürk E, Aktürk O Ü and Ciraci S 2016 *Phys. Rev. B* **94** 014115
[20] Feng B J, Sugino O, Liu R Y, Zhang J, Yukawa R, Kawamura M, Iimori T, Kim H, Hasegawa Y, Li H, *et al.* 2017 *Phys. Rev. Lett.* **118** 096401
[21] Li W B, Kong L L, Chen C Y, Gou J, Sheng S X, Zhang W F, Li H, Chen L, Cheng P and Wu K H 2018 *Sci. Bull.* **63** 282
[22] Wang Y X, Qiu G, Wang R X, Huang S Y, Wang Q X, Liu Y Y, Du Y C, Goddard III W A, Kim M J, Xu X F, Ye P D and Wu W Z 2018 *Nat. Electron.* **1** 228
[23] Ci L J, Song L, Jin C H, Jariwala D, Wu D X, Li Y J, Srivastava A, Wang Z F, Storr K, Balicas L, Liu F and Ajayan P M 2010 *Nat. Mater.* **9** 430
[24] Huang P, Riccardi E, Messelot S, Graef H, Valmorra F, Tignon J, Taniguchi T, Watanabe K, Dhillon S, Plaçais B, Ferreira R and Mangeney J 2020 *Nat. Commun.* **11** 863
[25] Zhang Y B, Tang T T, Girit C, Hao Z, Martin M C, Zettl A, Crommie M F, Shen Y R and Wang F 2009 *Nature* **459** 820
[26] Wang F, Zhang Y B, Tian C S, Girit C, Zettl A, Crommie M and Shen Y R 2008 *Science* **320** 206
[27] Bonaccorso F, Sun Z P, Hasan T and Ferrari A C 2010 *Nat. Photon.* **4** 611
[28] Baugher B W H, Churchill H O H, Yang Y F and Jarillo-Herrero P 2014 *Nat. Nanotechnol.* **9** 262
[29] Yu W J, Liu Y, Zhou H L, Yin A X, Li Z, Huang Y and Duan X F 2013 *Nat. Nanotechnol.* **8** 952
[30] Zanella I, Guerini S, Fagan S B, Mendes Filho J and Souza Filho A G 2008 *Phys. Rev. B* **77** 073404
[31] Ogawa S, Fukushima S and Shimatani M 2020 *Sensors* **20** 3563
[32] Fang Z Y, Liu Z, Wang Y M, Ajayan P M, Nordlander P and Halas N J 2012 *Nano Lett.* **12** 3808
[33] Luo L B, Zeng L H, Xie C, Yu Y Q, Liang F X, Wu C Y, Wang L and Hu J G 2014 *Sci. Rep.* **4** 3914
[34] Popov V V, Polischuk O V, Davoyan A R, Ryzhii V, Otsuji T and Shur M S 2012 *Phys. Rev. B* **86** 195437
[35] Nikitin A Y, Alonso-González P, Vélez S, Mastel S, Centeno A, Pesquera A, Zurutuza A, Casanova F, Hueso L E, Koppens F H L and Hillenbrand R 2016 *Nat. Photon.* **10** 239
[36] Rodrigo D, Limaj O, Janner D, Etezadi D, De Abajo F J G, Pruneri V and Altug H 2015 *Science* **349** 165
[37] Wu L, Chu H S, Koh W S and Li E P 2010 *Opt. Express* **18** 14395
[38] Anker J N, Hall W P, Lyandres O, Shah N C, Zhao J and Van D Richard P 2008 *Nat. Mater.* **7** 442
[39] Ouyang Q L, Zeng S W, Jiang L, Hong L Y, Xu G X, Dinh X Q, Qian J, He S, Qu J, Coquet P and Yong K T 2016 *Sci. Rep.* **6** 28190
[40] Wang C, Huang S Y, Xing Q X, Xie Y G, Song C Y, Wang F J and Yan H G 2020 *Nat. Commun.* **11** 1158
[41] Song C Y, Yuan X, Huang C, Huang S Y, Xing Q X, Wang C, Zhang C, Xie Y G, Lei Y C, Wang F J, Mu L, Zhang J S, Xiu F X and Yan H G 2021 *Nat. Commun.* **12** 386
[42] Jin F P, Roldán R, Katsnelson M I and Yuan S J 2015 *Phys. Rev. B* **92** 115440
[43] Ghosh B, Kumar P, Thakur A, Chauhan Y S, Bhowmick S and Agarwal A 2017 *Phys. Rev. B* **96** 035422
[44] Mannix A J, Zhou X F, Kiraly B, Wood J D, Alducin D, Myers B D, Liu X L, Fisher B L, Santiago U, Guest J R, *et al.* 2015 *Science* **350** 1513
[45] Feng B J, Zhang J, Zhong Q, Li W B, Li S, Li H, Cheng P, Meng S, Chen L and Wu K H 2016 *Nat. Chem.* **8** 563
[46] Zhou X F, Dong X, Oganov A R, Zhu Q, Tian Y J and Wang H T 2014 *Phys. Rev. Lett.* **112** 085502
[47] Dresselhaus M S, Dresselhaus G and Jorio A 2008 *Group theory: application to the physics of condensed matter* (Berlin: Springer Press)
[48] Hahn T 2005 *International Tables for Crystallography, Volume A* (Berlin: Springer Press)
[49] Lopez-Bezanilla A and Littlewood P B 2016 *Phys. Rev. B* **93** 241405
[50] Yuan J H, Yu N N, Xue K H and Miao X S 2017 *Rsc. Adv.* **7** 8654
[51] Sadhukhan K and Agarwal A 2017 *Phys. Rev. B* **96** 035410
[52] Jalali-Mola Z and Jafari S A 2018 *Phys. Rev. B* **98** 195415
[53] Jalali-Mola Z and Jafari S A 2018 *Phys. Rev. B* **98** 235430
[54] Zabolotskiy A D and Lozovik Y E 2016 *Phys. Rev. B* **94** 165403
[55] Zhang S H, Shao D F and Yang W 2019 *J. Magn. Magn. Mater.* **491** 165631
[56] Kong Z, Li J, Zhang Y, Zhang S H and Zhu J J 2021 *Nanomaterials* **11** 1462
[57] Zhu J J, Badalyan S M and Peeters F M 2013 *Phys. Rev. B* **87** 085401